



Numerical study on critical axial forces of upheaval buckling for initially stressed submarine pipelines on uneven seabed



Leige Xu^a, Mian Lin^{b,c,*}

^a School of Civil Engineering and Transportation, North China University of Water Resources and Electric Power, Zhengzhou, China

^b Institute of Mechanics, Chinese Academy of Sciences, Beijing, China

^c School of Engineering Science, University of Chinese Academy of Sciences, Beijing, China

ARTICLE INFO

Keywords:

The VFIFE method
Dimensional analysis
Upheaval buckling
Uneven seabed

ABSTRACT

For pipelines on uneven seabed, upheaval buckling may occur if the axial compressive force reaches the critical force of upheaval buckling. The critical axial force is sensitive to the seabed undulation. However, the effect of the seabed undulation on the critical force has not been completely discussed. Moreover, effect of the initial stress which accumulates in the pipe wall when the pipeline conforms to the seabed undulation under self-weight has been rarely examined. This paper mainly focuses on the effect of the initial stress. Using numerical tools developed with the Vector Form Intrinsic Finite Element (VFIFE) method, effect of the initial stress is proved significant. Subsequently with the theory of dimensional analysis, a formula of the critical axial force is derived. This formula covers the dimensionless undulation length and the Out-of-Straight (OOS) of the seabed undulation. Considering three seabed undulation shapes, coefficients in the formulas are determined with numerical results from the VFIFE simulations. Finally, the proposed formulas are proved applicable for pipes with different properties and within the error range of $\pm 10\%$ for pipelines in continuous contact with the seabed in a large dimensionless scope.

1. Introduction

When a pipeline is laid on topography with uneven seabed, it may buckle vertically once the axial compressive force is larger than a value called the critical axial force of upheaval buckling (Guijt, 1990; Liu et al., 2012a, 2012b; Palmer et al., 1990; Wang et al., 2015). Upheaval buckling is a failure mode and may result in cross-sectional distortion or rupture of the pipe (Croll, 1997; Liu et al., 2014b). And because of the economic losses and environmental damage resulted from possible pipeline leaks, upheaval buckling must be considered in design and in-service assessment of pipelines. As upheaval buckling happens only when the axial compressive force of the pipeline reaches the critical value, designers could prevent its happening by keeping the axial force smaller than the critical axial force of upheaval buckling (Xu and Lin, 2017c). Therefore, it will help much in practice if the critical axial force could be predicted with a great precision.

For pipelines on uneven seabed, the seabed undulation may trigger upheaval buckling of the pipeline. For a pipeline on seabed with undulation, two situations are considered: the situation with initially unstressed pipe (Fig. 1(a)) and the situation with initially stressed pipe

(Fig. 1(b)). Fig. 1(a) corresponds to local undulation in the pipe itself with a conforming seabed. The undulation of the pipeline profile may result from the residual curvature in the pipe-laying process (Liu et al., 2012a; O'Grady and Harte, 2013) or the snaked-laying of the pipeline (Guan et al., 2007; Liu et al., 2012b). Fig. 1(b) represents the undulation in the seabed with a bending pipeline, which is initially straight and has to bend under submerged weight to conform to the seabed undulation (Liu et al., 2012a). For a typical seabed undulation, the maximum cross-sectional stress contours of the pipeline segments are also shown in Fig. 1. It is illustrated that there is no initial stress in an initially unstressed pipe, while in an initially stressed pipe, the initial stress is significant.

Many researches have been conducted to study the critical upheaval buckling forces of submarine pipelines. Yun and Kyriakides (1985) studied the upheaval buckling of buried pipelines through a large deflection extensional beam nonlinear formulation. They found the critical axial forces are sensitive to undulation of the pipeline profile. Taylor et al. (Taylor and Gan, 1986, 1987; Taylor and Tran, 1993, 1996) studied the upheaval buckling of unstressed pipelines through theoretic analysis and experiments. They manifested the undulation length L and

* Corresponding author. Institute of Mechanics, Chinese Academy of Sciences, Beijing, China.
E-mail address: linmian@imech.ac.cn (M. Lin).

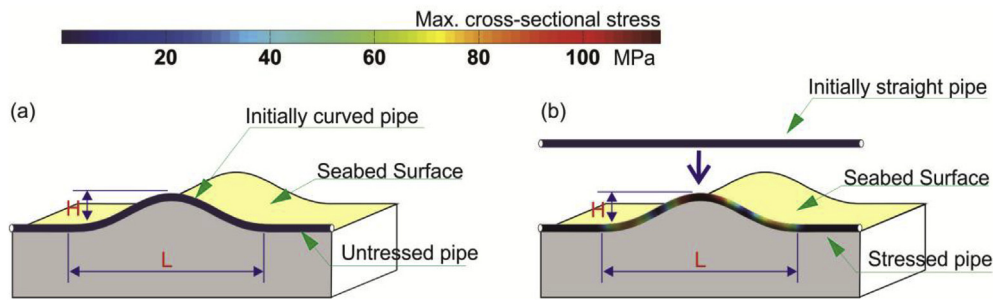


Fig. 1. Schematic diagram of (a) an initially unstressed pipeline, and (b) an initially stressed pipeline, laid on seabed with undulation.

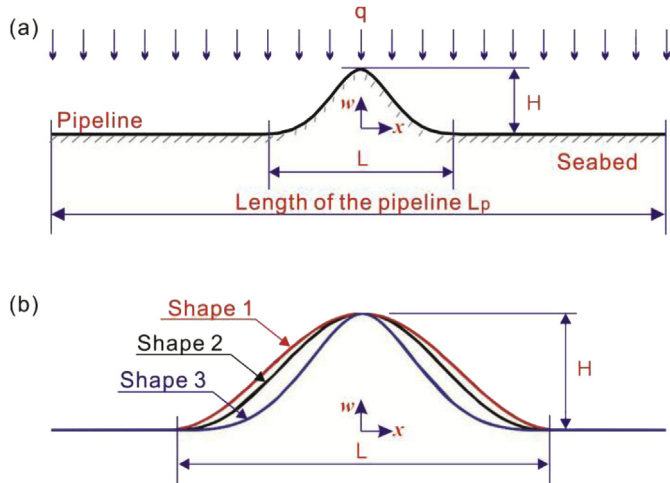


Fig. 2. (a) The analytical model, and (b) diagram of three typical seabed undulation shapes.

Table 1
Parameters of the studied pipe.

Property	Value
The outer diameter, D (mm)	457
The thickness of the steel pipe wall, t (mm)	14.3
The Young's modulus, E (GPa)	207
The Poisson's ratio, ν	0.3
The equivalent cross-sectional moment of inertia, I (m^4)	4.88×10^{-4}
The equivalent cross-sectional area, A (m^2)	0.0199
The distributed load on pipelines, q (N/m)	1 500
The thermal expansion coefficient, α_s ($1/^\circ C$)	1.17×10^{-5}

height H can influence the critical axial force. Richards (1990) studied the influence of undulation shape on upheaval buckling behavior of initially unstressed pipeline and proved this influence is significant. Based on this, he pointed out the seabed profile survey is important for the pipeline design process. Assuming the buckling mode of a pipeline segment is the growth of the periodic initial mode, Maltby and Calladine (1995a,b) proposed formulas for the critical axial force including the undulation amplitude. Croll (1997, 1998) deduced analytical expressions of the upper and lower bounds of the critical axial force, while the length and height of the undulation are separating in the equations.

Palmer et al. (1990) introduced a semi-empirical simplified design method and presented the general form of the critical force formulas. They proved the specific undulation shape only affects the coefficients of the formulas, while the general form of the formulas keeps unchanged. This provided basis for the using of the theory of dimensional analysis in this problem. With the theory of dimensional analysis and finite element analysis, Zeng et al. (2014) studied the influences of the Out-of-straightness (OOS) and the undulation shape for initially

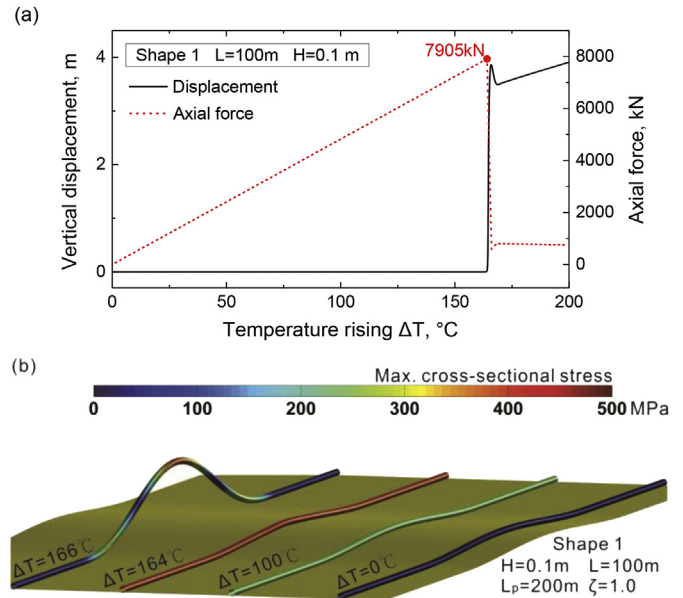


Fig. 3. (a) Temperature rising versus the vertical displacement and axial force; (b) the maximum cross-sectional stress and deformation contour plot at different temperatures (shape 1, $H = 0.1$ m, $L = 100$ m, $\zeta = 1.0$).

unstressed pipelines. Again, it was proved that the form of the critical axial force formulas is the same for different undulation shapes. However, effect of the imperfection size was not systematically considered in Zeng et al. (2014). To account for this size effect, Xu and Lin (2017c) proposed a new dimensionless parameter, the dimensionless imperfection length, which combines the effects of the imperfection length, the bending stiffness and vertical load of the pipeline. Moreover, approximation formulas covering the dimensionless imperfection length and the OOS were proposed by Xu and Lin (2017c). However, in the study of Xu and Lin (2017c), pipelines are assumed to be initially curved and with no initial stress.

Although the stressed pipeline and the unstressed pipeline are both common in practice, there are few researches about initially stressed pipeline, for which the bending stress caused by the seabed undulation must be considered. For a long-distance pipeline through sand-wave topography, Xu and Lin (2017b) studied the influence of the initial stress caused by real seabed undulations and found the stress is considerable and could significantly influence behaviors and internal forces of free-spanning pipelines. Karampour et al. (2013) derived a tabulated analytical solution based on a long heavy elastic beam resting on a rigid seabed for both stressed and unstressed pipelines. They found the critical axial force of initially stressed pipeline is larger than that of the initially unstressed pipeline. This indicates it may be over-conservative to directly adopt the results of the initially unstressed pipeline in the initially stressed situation. Nevertheless in previous studies, effects of the initially

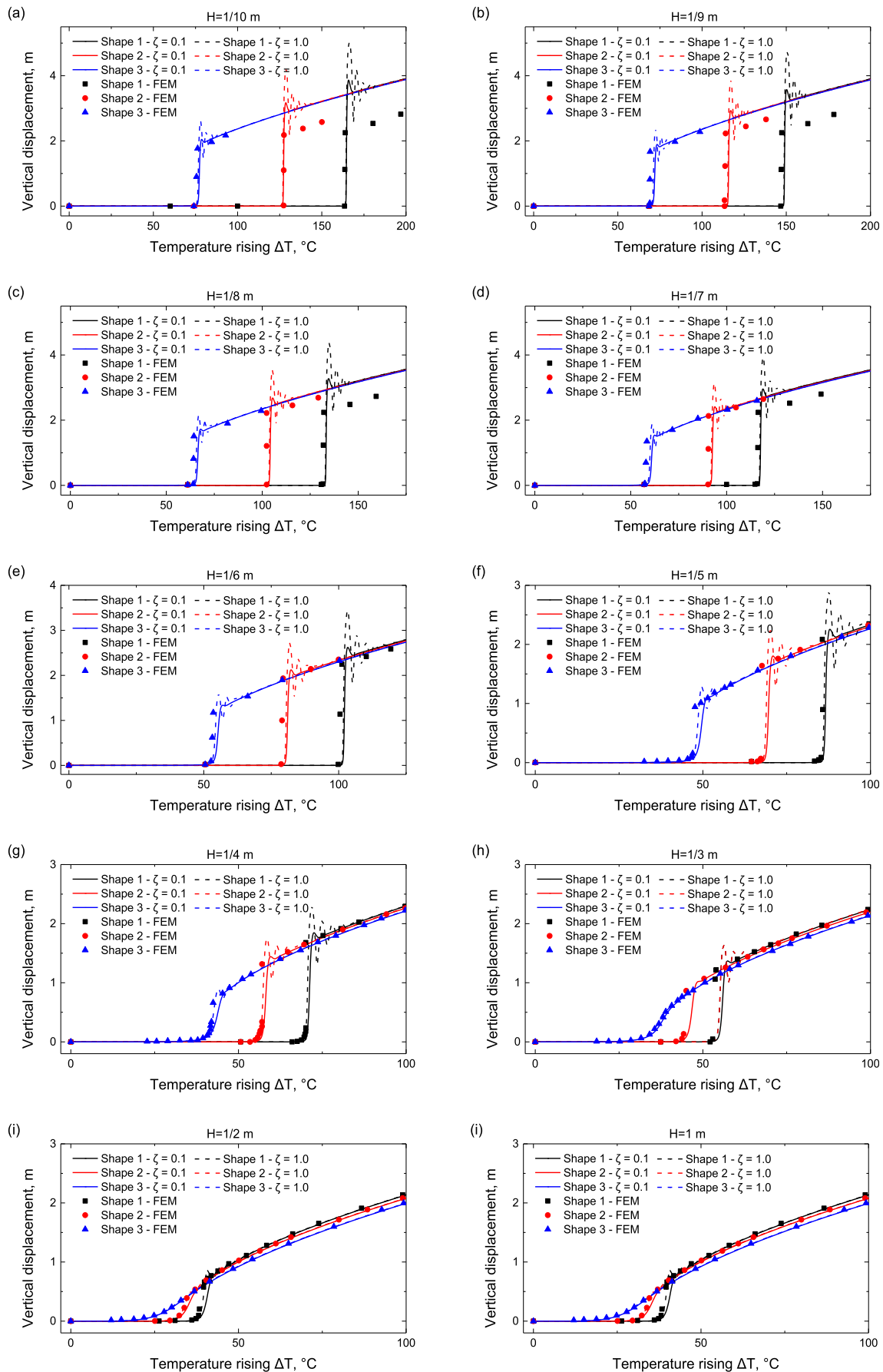


Fig. 4. Temperature rising versus vertical displacement from the VFIFE simulations and FEM results in Zeng et al. (2014).

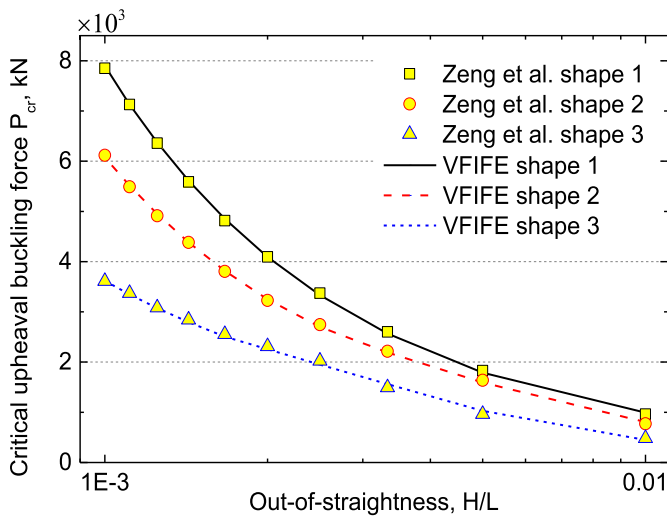


Fig. 5. Comparison between the critical axial forces using the VFIFE method and FEM (Zeng et al., 2014) for initially unstressed pipelines.

stress is not well studied.

The present paper mainly focuses on the initially stressed pipelines. Firstly, numerical simulations are conducted with the Vector Form Intrinsic Finite Element (VFIFE) method. The numerical results of the VFIFE method are compared with those of the conventional FEM. Subsequently, effect of the initial stress caused by the seabed undulation is discussed. And amounts of simulations are conducted with three seabed undulation shapes. Moreover, with dimensional analysis and the numerical results, useful fitting formulas are presented. Finally, the proposed formulas are compared with numerical results for different types of pipes. By this way, the dimensionless application scopes of the proposed formulas are determined.

2. Numerical model and verification

In this section, the VFIFE model used in this study will be briefly introduced. Subsequently, the initially unstressed pipeline is simulated using the VFIFE model and the results are compared with traditional FEM results in previous research. After this, effect of the initially stress caused by the seabed undulation is discussed.

2.1. The VFIFE model

The Vector Form Intrinsic Finite Element (VFIFE) model used in this paper was originally developed by Xu and Lin (2014) and are amongst the first applying the VFIFE method to pipelines. The VFIFE model was developed using FORTRAN program and the postprocessor is developed based on MATLAB platform. Xu and Lin (2014) proved the VFIFE model is as accurate as traditional FEM in simulating of free-spanning pipelines. In their study, the VFIFE method was integrated with the UWAPIPE model (Tian and Cassidy, 2010; Youssef et al., 2013) to consider the complicated pipe-soil interaction. When applying the VFIFE model to long-distance pipelines, the computing amount is considerable. Therefore, Xu and Lin (2017b) proposed a high-efficiency Message Passing Interface (MPI) parallel scheme suitable for the VFIFE method and developed the MPI-parallel VFIFE procedure. Using the procedure, they simulated the configuration of a 10 km long-distance pipeline lying on a real irregular seabed and proved the VFIFE model is a useful tool for simulation of long-distance pipelines. To study the potential failure positions and plastic deformation of pipelines subjected to active faults, Liu et al. (2016a) developed the procedure by incorporating the VFIFE method with fiber element model. Furthermore, Xu and Lin (2017a) proposed a beam-shell coupling scheme based on the VFIFE method to

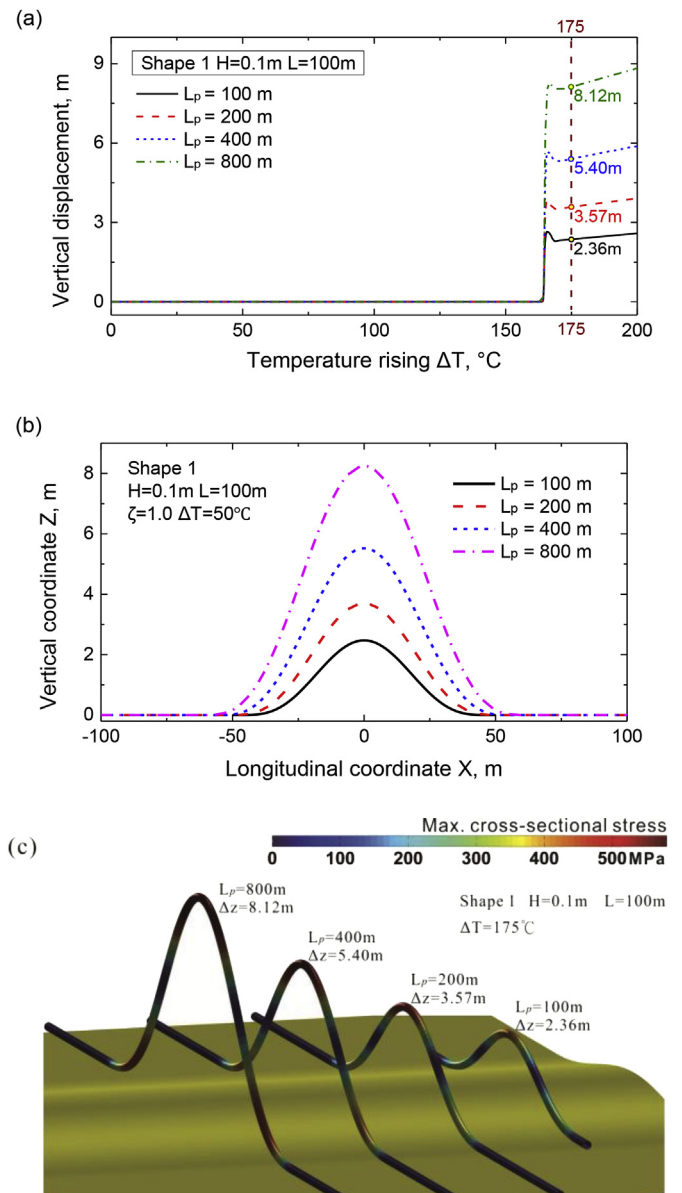


Fig. 6. (a) Temperature rising versus vertical displacement; (b) distribution of the vertical displacement along the longitudinal direction; (c) the maximum cross-sectional stress and deformation contour plot at $\Delta T = 175^{\circ}C$ for cases with different modeled pipeline length (shape 1, $H = 0.1$ m, $L = 100$ m, $\zeta = 1.0$).

simulate local buckling of long-distance pipelines crossing active faults. A MPI parallel procedure using the beam-shell coupling scheme was also developed and numerical results shows that the procedure is both efficient and accurate for analysis of long-distance pipelines. Most recently, Xu and Lin (2017c) studied upheaval buckling of initially unstressed imperfect pipelines and proved the VFIFE model is as accurate as traditional Finite Element Method (FEM) in global buckling analysis of pipelines.

In the VFIFE model, the equivalent longitudinal force caused by the internal pressure and temperature can be obtained following Fan (2013) as

$$\Delta f_{T+p} = EA\alpha\Delta T + \frac{\pi}{4}(1 - 2\nu)(p_i D_i^2 - p_o D_o^2) \quad (1)$$

where, Δf_{T+p} is the equivalent longitudinal force caused by internal pressure and temperature; ΔT is the temperature variation; D_i and D_o are the equivalent inner diameter and outer diameter, respectively; p_i and p_o

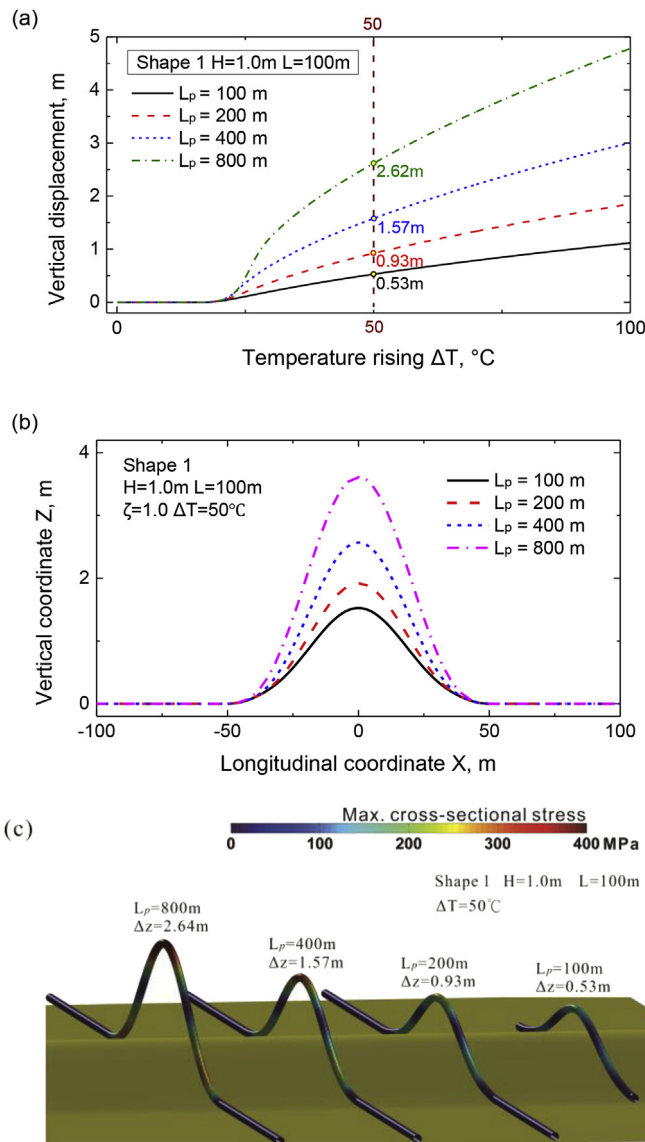


Fig. 7. (a) Temperature rising versus vertical displacement; (b) distribution of the vertical displacement along the longitudinal direction; (c) the maximum cross-sectional stress and deformation contour plot at $\Delta T = 50$ °C for cases with different modeled pipeline length (shape 1, $H = 1.0$ m, $L = 100$ m, $\zeta = 1.0$).

are the internal pressure and the outer pressure of the pipe respectively; E , ν and A are the elastic modulus, the Poisson's ratio and the cross-sectional area of the pipe.

2.2. Verification of the VFIFE model

Zeng et al. (2014) and Xu and Lin (2017c) studied the buckling of the initially unstressed pipeline. The analytical model is illustrated in Fig. 2(a). Similar analytical models have been used by other researchers (Taylor and Tran, 1993; Zeng et al., 2014; Zhang and Duan, 2015). Three different imperfection shape functions ($f_1 - f_3$) are assumed to account for possible undulations of the seabed following (Xu and Lin, 2017c; Zeng et al., 2014). The three functions are presented as follows.

Shape 1

$$f_1(x) = \frac{H}{2} \left(1 + \cos\left(\frac{2\pi x}{L}\right) \right), \quad -\frac{L}{2} \leq x \leq \frac{L}{2} \quad (2)$$

Shape 2

$$f_2(x) = \begin{cases} H \left(\frac{8}{3} \left(\frac{2x}{L} \right)^2 + 3 \frac{2x}{L} + 1 \right) \left(1 - \frac{2x}{L} \right)^3, & 0 \leq x \leq \frac{L}{2} \\ H \left(\frac{8}{3} \left(\frac{2x}{L} \right)^2 - 3 \frac{2x}{L} + 1 \right) \left(1 + \frac{2x}{L} \right)^3, & -\frac{L}{2} \leq x < 0 \end{cases} \quad (3)$$

Shape 3

$$f_3(x) = \begin{cases} H \left(4 \frac{2x}{L} + 1 \right) \left(\frac{2x}{L} - 1 \right)^4, & 0 \leq x \leq \frac{L}{2} \\ -H \left(4 \frac{2x}{L} - 1 \right) \left(\frac{2x}{L} + 1 \right)^4, & -\frac{L}{2} \leq x < 0 \end{cases} \quad (4)$$

where H and L are the height and length of the seabed undulation, respectively; x is the coordinate in the longitudinal direction. The curves corresponding to the above functions are drawn in Fig. 2(b). The pipeline properties are given in Table 1.

A series of numerical cases are carried out to verify the VFIFE model. Following Zeng et al. (2014), the initial curvature of a pipeline is the same with the seabed surface profile and the pipeline is therefore initially unstressed. Ten simulations with different OOS from 0.001 to 0.01 are performed for each seabed shape. In the simulations, the undulation length L is 100 m and the pipeline length is 200 m. The loading time of the simulation is as long as 300s, this could ensure the pipeline is in quasi-static condition before upheaval buckling. The element discretization of the pipeline is uniform with element length of 1 m and the time increment is $dt = 5.0 \times 10^{-5}$ s. The internal flow temperature of the pipeline at initial time $t = 0$ is 10 °C, with a linear increasing, the temperature reaches at 210 °C at the ending of the loading process (at $t = 300$ s). The thermal expansion coefficient of pipe steel is $\alpha_s = 1.17 \times 10^{-5} / ^\circ\text{C}$ as listed in Table 1.

The axial stress caused by temperature rising is $\sigma = E\alpha_s\Delta T$. The axial stress corresponding to the maximum temperature rising of 200 °C is 484 MPa, which is a value comparable to the yield stress of most kinds of pipe steel. The mechanism of plastic buckling is different with that of elastic buckling and most of upheaval buckling happens within the elastic range. Aiming at proposing approximation formulas with more simple forms, plastic buckling is not considered in the present study. And correspondingly, the pipe steel is assumed to be elastic.

Tomes et al. (1997) indicated that for a given undulation, the critical axial force required to buckle the pipeline is constant and independent of the level of the axial seabed friction. Karampour et al. (2013) manifested the effect of axial seabed friction on upheaval buckling is only evident in the post-buckling stage. Therefore in this research, the friction ratio between the pipe and the foundation is set as zero.

When the undulation height $H = 0.1$ m, the vertical displacement curve and axial force curve of the pipeline segment's middle point are plotted in Fig. 3(a). A big displacement suddenly appears at the critical temperature and the corresponding axial force are called the critical axial force. As shown in Fig. 3, upheaval buckling happens at the temperature rising of 165 °C and the critical axial force is 7 905 kN. A series of simulations are conducted and the results are shown in Figs. 4 and 5, where the critical axial forces from the VFIFE simulations are compared to those of FEM in Zeng et al. (2014). The maximum relative difference is about 3%. The accuracy of the VFIFE procedure is therefore proved acceptable in analysis of pipeline upheaval buckling. Refer to Xu and Lin (2017c) for more details about verification of the VFIFE model.

Similar to the findings in Liu et al. (2012a), energy transfers from elastic energy to kinematic energy when upheaval buckling happens. As shown in Fig. 3, before upheaval buckling, axial compressive stress accumulates in the pipe wall because of thermal expansion. Accordingly, elastic energy in the pipeline increases. At the onset of upheaval buckling, the elastic energy in the pipeline releases and transfers into kinematic energy of the pipeline. Correspondingly, the pipeline vibrates in the vertical direction. As shown in Fig. 4, the axial force and vertical

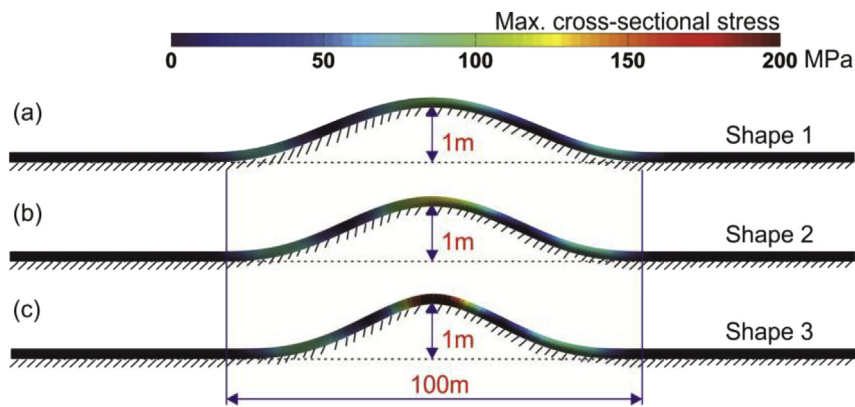


Fig. 8. The maximum cross-sectional stress and deformation contour plot after the in-place simulation: (a) shape 1, (b) shape 2, and (c) shape 3.

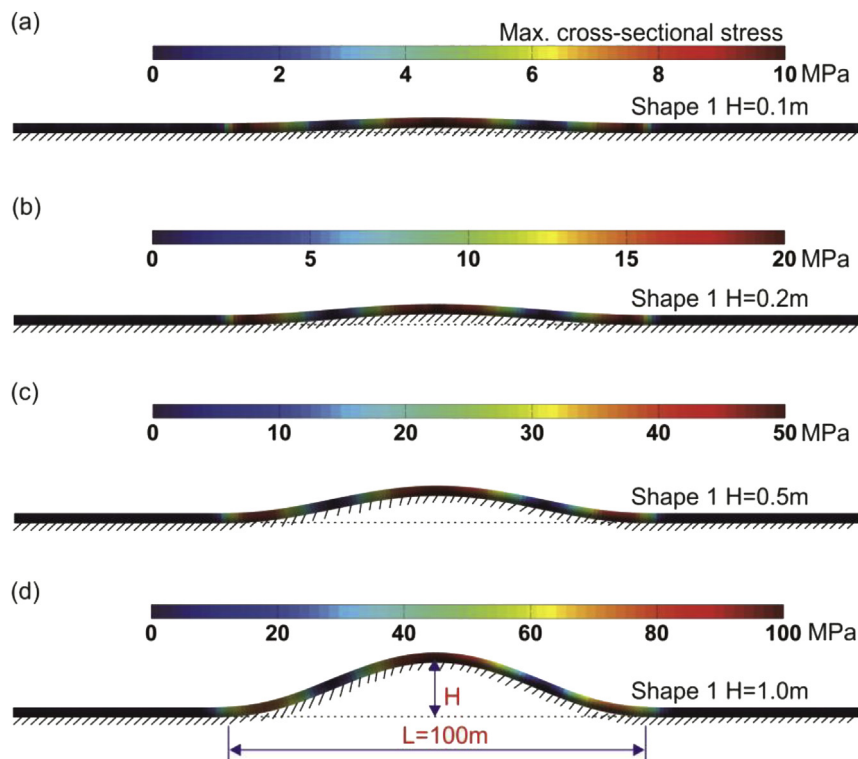


Fig. 9. The maximum cross-sectional stress and deformation contour plot after the in-place simulation: (a) $H = 0.1$ m, (b) $H = 0.2$ m, (c) $H = 0.5$ m, and (d) $H = 1.0$ m.

displacement of the pipeline oscillates after upheaval buckling when the damping ratio is $\zeta = 0.1$.

Before upheaval buckling, the pipeline is in quasi-static condition and after upheaval buckling, the pipeline is in dynamic responses. In a structural dynamic response analysis, the damping ratio could significantly influence the results, whilst in a quasi-static analysis, structural responses was hardly influenced by the damping ratio (Xu and Lin, 2017c). Therefore, the damping ratio hardly influence the critical axial force of upheaval buckling. And larger the damping ratio is, more stable the post-buckling responses will be. When the damping ratio is $\zeta = 1.0$, the post-buckling behaviors of the pipelines are almost quasi-static and correspondingly in the displacement curves, there is no oscillation but just a little jump. Therefore, a relatively larger structural damping ratio of $\zeta = 1.0$ is used in this paper to obtain more stable post-buckling behaviors.

Notably, Fig. 4(a–d) shows that when the vertical displacement is larger than about 2.0 m, the post-buckling displacement of the VFIFE results diverges with that of FEM in (Zeng et al., 2014). The possible reason of this difference may be that in the VFIFE simulations, the

pipeline is assumed to be elastic and the plastic deformation is not considered. In future study on the post-buckling behaviors, the plastic effect must be considered.

Sensitivity analysis has been conducted to determine the modeled pipeline length. As shown in Figs. 6 and 7, the modeled pipeline length hardly influence the critical axial force of upheaval buckling but has great influence on the post-buckling behaviors. Zhu et al. (2015) have drawn the same conclusion that the length of the modeled pipeline hardly influence the critical condition of global buckling. Meanwhile, Liu et al. (2016b; 2014b) suggested that the modeled pipeline length could greatly influence the post-buckling behaviors. It can be seen from Figs. 6 and 7 that longer the modeled pipeline is, more dramatic the post-buckling behavior will be. And correspondingly, it will be more accurate to identify the onset of upheaval buckling. However, longer the modeled pipeline is, more computing expensive it will be. In this paper, the overall length of the modeled pipeline is determined as $4L$, where L is the imperfection length.

The displacement distribution shown in Fig. 7(b–c) and 8 (b–c) could

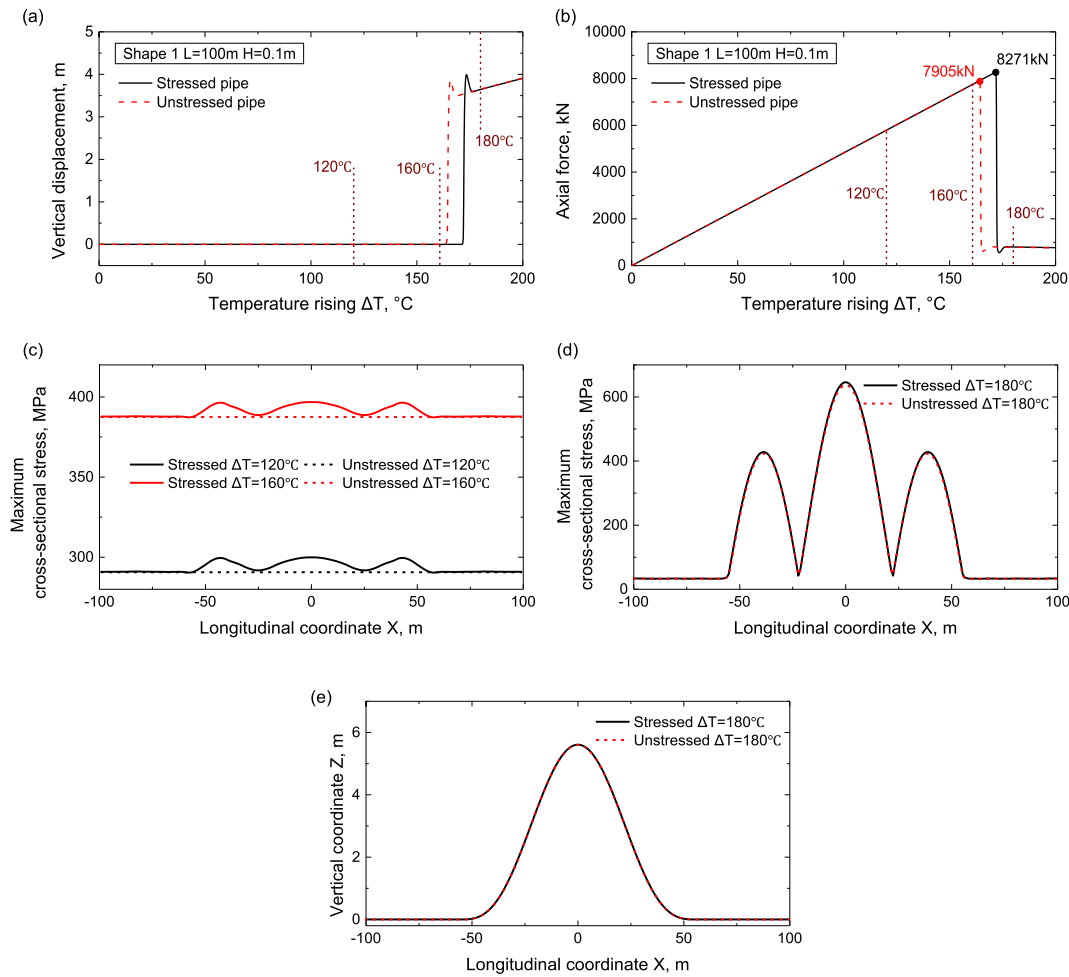


Fig. 10. (a) Temperature rising versus vertical displacement curves, (b) temperature rising versus axial force curves, (c) maximum cross-sectional stress profiles before upheaval buckling, (d) maximum cross-sectional stress profiles after upheaval buckling and (e) vertical coordinate profiles ($H = 0.1$ m).

also represent the buckling mode of the pipelines. The buckling mode is in accordance with the study of Wang et al. (2015). In this paper, two kinds of ends' constraints have been considered: hinged and fixed. When hinged, no translation is permitted at both ends and when fixed, no translation and rotation is permitted. Interestingly, it is found that the influence of the ends' constraints is negligible. The reason is that the pipeline has no rotation at the ends even if the ends are hinged, as shown in Fig. 7 (b–c) and 8 (b–c).

2.3. Effect of initial stress

As mentioned in the introduction, the critical axial forces of the initially stressed and unstressed pipelines may differ greatly. In order to investigate this difference, a series of simulations are conducted with each seabed shape. Different from the loading process of the initially unstressed pipeline, for the initially stressed situation, an in-place simulation process is conducted before the thermal expansion process. At time $t = 0$ s, a straight pipeline is placed above the seabed undulation as shown in Fig. 1(b). Gravity of the pipeline is applied and the pipeline moves downward to the seabed at a velocity kept lower than 0.02 m/s. This velocity will ensure the in-place simulation process is in approximately quasi-static condition. In the simulation, the seabed is assumed to be a rigid surface and this is a common assumption in previous analytical methods (Liu et al., 2014a; Wang et al., 2015; Zeng et al., 2014; Zhang and Duan, 2015). After the in-place process, both ends of the pipeline are then fixed and the same thermal rising process for the unstressed pipeline

in section 2.2 follows.

Fig. 8 shows the maximum cross-sectional stress and deformation of pipeline segments on seabed with different shapes of undulations after the in-place simulation. When the undulation length $L = 100$ m and height $H = 1.0$ m, the maximum cross-sectional stress in the pipeline segments are very dramatic and differs with the undulation shape. Moreover, as shown in Fig. 9, the initial stress increases with the undulation height when the undulation length is constant.

When the undulation height $H = 0.1$ m, the vertical displacement curve and the axial force curve are shown in Fig. 10(a–b). When the undulation height $H = 1.0$ m, the corresponding curves are shown in Fig. 11(a–b). It is illustrated that the initial stress has the effect of stabilizing the pipeline segment. The critical temperature and critical axial force are both larger for the stressed cases. Figs. 10(c) and 11(c) shows the maximum cross-sectional stress profiles of the stressed and unstressed pipelines before upheaval buckling. The stress profiles of the stressed pipelines combine the axial thermal stress and the bending stress, whilst the stress profiles of the unstressed pipelines account for only the axial thermal stress. Fig. 10 (d) shows that the stress profiles of the stressed pipeline and the unstressed pipeline are similar. The reason could be found in Fig. 10 (e), which shows that the displacement profiles of the stressed and unstressed pipelines are almost the same in this situation. However when the imperfection height is 1.0 m, Fig. 11(d–e) show that both the stress profiles and the displacement profiles of the stressed pipelines and unstressed pipelines are very different. This is because that the influence of the initial stress increases with imperfection height.

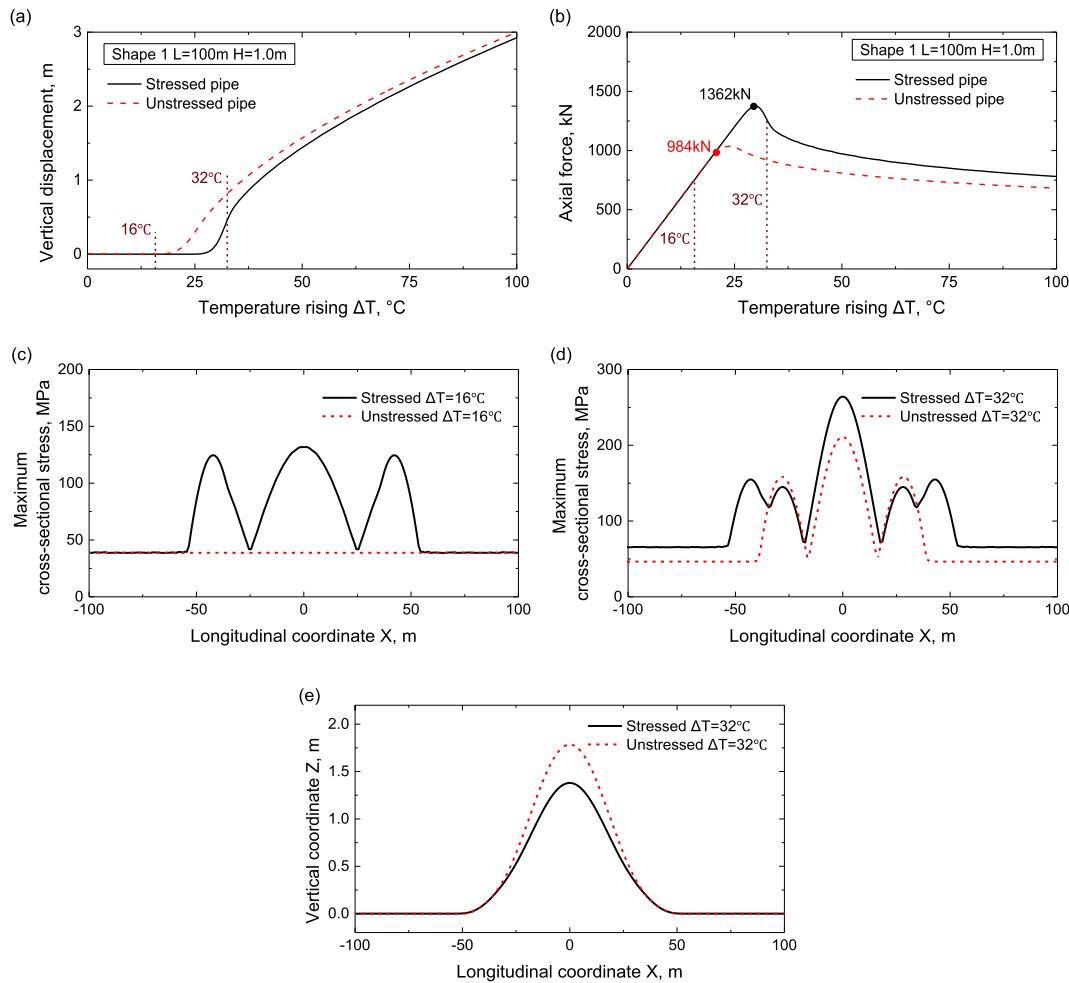


Fig. 11. (a) Temperature rising versus vertical displacement curves, (b) temperature rising versus axial force curves, (c) maximum cross-sectional stress profiles before upheaval buckling, (d) maximum cross-sectional stress profiles after upheaval buckling and (e) vertical coordinate profiles ($H = 1.0$ m).

The critical axial forces of the initially stressed and unstressed pipelines are compared in Fig. 12. For the three seabed shapes, the critical forces of the initially stressed pipelines are all larger than the ones of the initially unstressed pipelines. Define the relative differences as

$$R_p = \frac{P_{cr}^s - P_{cr}^u}{P_{cr}^s} \times 100\% \quad (5)$$

where R_p is the relative difference, P_{cr}^s is the critical force of the initially stressed pipeline and P_{cr}^u is the critical force of the initially unstressed pipeline. Fig. 12(d) shows the relative difference R_p . The relative difference increases with larger OOS and with more compacted seabed shapes. The minimum relative difference is 6% with $H/L = 0.001$ for shape 1, and the maximum relative difference is 70% with $H/L = 0.01$ for shape 3. For pipeline on foundations with larger OOS and more compacted foundation shapes, the pipeline bend more severely and the pipe-wall stresses are larger as shown in Fig. 8. As in the unstressed situation, there is no initial bending stress in the pipe-wall, the differences between the two stressed and unstressed situations are mainly resulted from the initial pipe-wall stress. Therefore, the relative difference is larger with larger OOS and more compacted foundation shapes. To conclude, the influence of initial pipe-wall stress is significant and it will be over-conservative to directly adopt the results of the unstressed pipeline in the stressed situation. In the following paper, we will focus on the initially stressed pipeline.

3. Dimensional analysis

Based on the Euler buckling theory and the previous research on pipeline upheaval buckling problem (Palmer et al., 1990; Taylor and Tran, 1996), Zeng et al. (2014) proposed approximation formulas for initially unstressed imperfect pipelines. In the formulas, influence of the OOS of an imperfection is considered. Recently, Xu and Lin (2017c) further developed the approximation formulas of initial unstressed imperfect pipelines by bringing in a new dimensionless parameter, the dimensionless imperfection length, to account for the size effect of an pipeline undulation.

Although the above researches are all about initially unstressed pipelines, while the dimensional analysis in the above researches are also applicable for the initially stressed cases. Following the dimensional analysis in Xu and Lin (2017c), in this paper, the critical axial force is function of EI , q , H and L :

$$P_{cr} = f(EI, q, H, L) \quad (6)$$

where P_{cr} is the critical axial force; H and L are the height and length of the undulation, respectively; q is the vertical distributed force, which is the submerged weight of a pipeline in the present study; EI is the bending stiffness of the pipeline.

In the above equation, dimensions are $[P_{cr}] = F$, $[EI] = FL^2$, $[q] = F/L$, $[H] = L$ and $[L] = L$. There are 5 physical quantities and 2 independent dimensions, so there must be 3 dimensionless independent quantities. Normalize the critical force P_{cr} with the critical buckling force of a

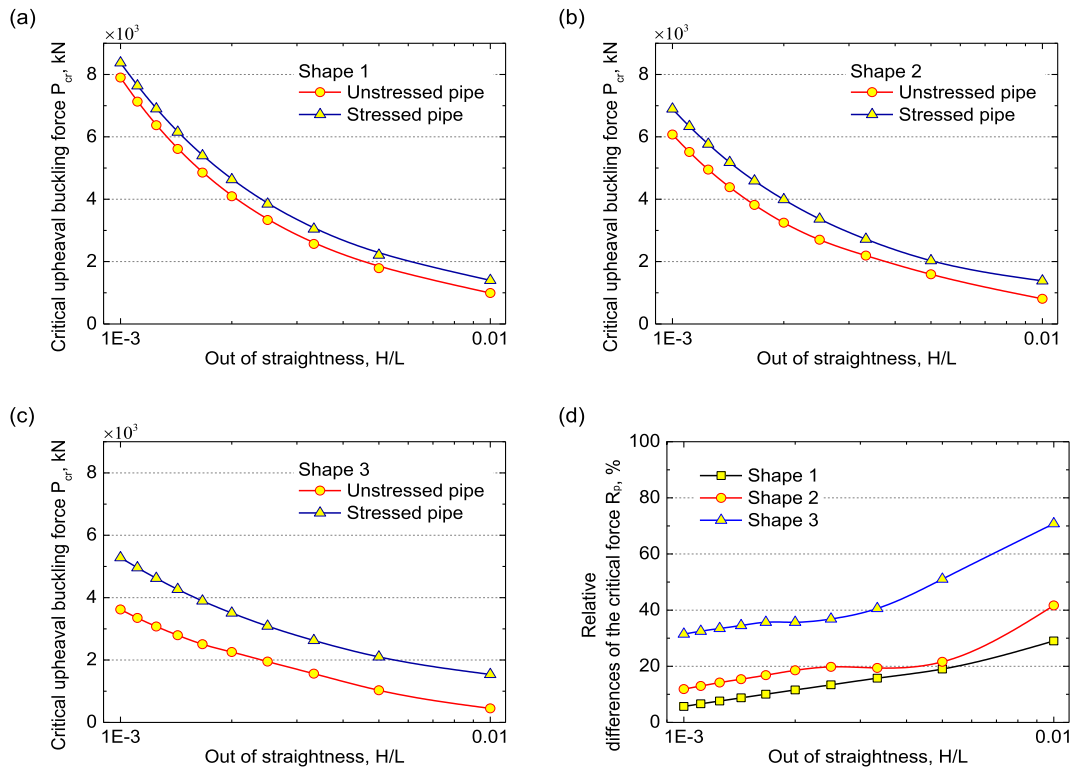


Fig. 12. Comparison between the critical axial forces of the initially stressed and stressed pipelines with different seabed shapes: (a) shape 1, (b) shape 2, (c) shape 3, and (d) the relative differences.

straight compressed column, the dimensionless critical axial force \bar{P}_{cr} is obtained:

$$\bar{P}_{cr} = \frac{P_{cr}L^2}{EI} \quad (7)$$

Another dimensionless quantity is the OOS H/L . Normalize the undulation length L with EI and q , the dimensionless undulation length \bar{L} can be obtained as

$$\bar{L} = L \left(\frac{q}{EI} \right)^{\frac{1}{3}} \quad (8)$$

According to the Buckingham's Pi-theorem (Tan, 2011), the above three dimensionless independent quantities can form definite relationship that reflect the substance of the problem,

$$\bar{P}_{cr} = f \left(\bar{L}, \frac{H}{L} \right) \quad (9)$$

When processing numerical results, independent variables can divide into different application ranges and a power formula can be adopted in each application range (Tan, 2011), therefore we assume:

$$\bar{P}_{cr} = C \bar{L}^\alpha \left(\frac{H}{L} \right)^\beta \quad (10)$$

After logarithm transition, we get

$$\log \bar{P}_{cr} = \log C + \alpha \log \bar{L} + \beta \log \frac{H}{L} \quad (11)$$

The above equation indicates the dimensionless quantities were assumed to meet the linear relationship in logarithmic form. This assumption will be verified in the next section.

4. Results and discussion

4.1. Results

To fit the coefficients in Eqs. (10) and (11), totally 36 simulations are performed for each seabed shape. The undulation length and height are listed in Table 2. Each case is represented by a scatter point in Fig. 13. The horizontal axis and the vertical axis are the height H and length L of the seabed undulation, respectively. The simulations are divided into four groups (group 1, group 2, group 3, and group 4). For the simulation in group 1, the undulation length L is 100 m and the undulation height H is respectively 1 m, 1/2 m, 1/3 m, ..., 1/10 m. In group 2, the OOS H/L is 0.01 and the undulation length L is respectively 80 m, 90 m, 100 m, ..., 200 m. In group 3, the undulation length L is 200 m, and the undulation height H is respectively 0.2 m, 0.4 m, 0.6 m, ..., 2 m. In group 4, the OOS H/L is 0.001 and the undulation length L is respectively 50 m, 75 m, 100 m, ..., 200 m.

The critical axial forces of all the cases are listed in Table 2. Fig. 14 plots the dimensionless critical axial forces in logarithmic form with $L = 100$ m (group 1, $\bar{L} = 2.4584$) and $L = 200$ m (group 3, $\bar{L} = 4.9176$). For the results with two undulation lengths and three shapes, the dimensionless critical forces and the out-of-straightness meet the linear relationship in logarithmic form, this consists with Eq. (11). Besides, the slope angles decrease with more compacted seabed shape, this suggest the coefficient β in Eq. (11) are different for different undulation shapes.

To discuss the influence of undulation length L on the pipeline critical axial force when H/L is constant, two series of simulations are carried out with the OOS $H/L = 0.01$ (group 2) and $H/L = 0.001$ (group 4). The dimensionless results are shown in Fig. 15 in logarithmic form. The dimensionless axial force increases linearly with the dimensionless undulation length. For different shapes, the slope angles are also different, which means that the coefficient α in Eqs. (10) and (11) are different for the three undulation shapes.

Table 2
The VFIFE results of the critical axial forces used to fit Eqs. (18)–(20).

Case parameters			Critical axial forces P_{cr} (kN)		
No.	Height H (m)	Length L (m)	Shape 1	Shape 2	Shape 3
1	0.8	80	1394	1350	1676
2	0.9	90	1362	1289	1548
3	1.0	100	1347	1287	1472
4	1.1	110	1368	1288	1396
5	1.2	120	1395	1280	1343
6	1.3	130	1419	1285	1302
7	1.4	140	1455	1301	1264
8	1.5	150	1507	1325	1239
9	1.6	160	1556	1344	1222
10	1.7	170	1607	1367	1201
11	1.8	180	1660	1396	1184
12	1.9	190	1720	1429	1171
13	2.0	200	1780	1465	1159
14	1/9	100	7646	6353	4987
15	0.125	100	6914	5788	4648
16	1/7	100	6170	5202	4295
17	1/6	100	5415	4611	3924
18	0.2	100	4638	4001	3529
19	0.25	100	3856	3377	3106
20	1/3	100	3051	2726	2643
21	0.5	100	2214	2038	2114
22	0.05	50	6011	5753	6472
23	0.075	75	7094	6184	5653
24	0.1	100	8392	6917	5313
25	0.125	125	9742	7733	5176
26	0.15	150	11,101	8491	5142
27	0.175	175	12,376	9182	5118
28	0.2	200	–	9728	5050
29	0.4	200	7299	5536	3280
30	0.6	200	5086	3992	2523
31	0.8	200	3949	3146	2102
32	1.0	200	3253	2622	1830
33	1.2	200	2780	2263	1634
34	1.4	200	2438	2001	1486
35	1.6	200	2177	1799	1369
36	1.8	200	1970	1639	1274

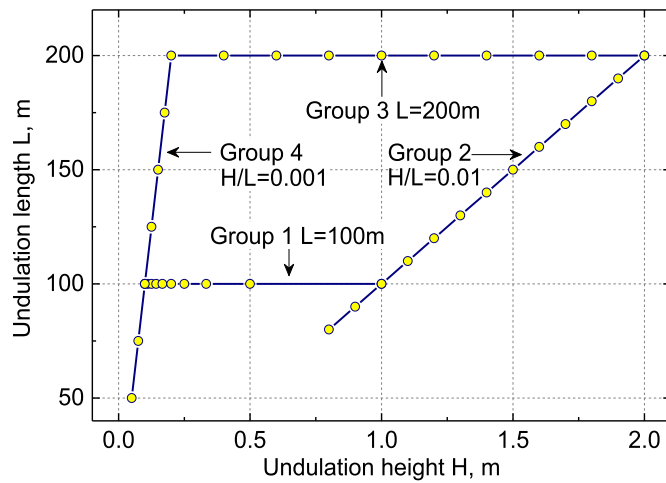


Fig. 13. The length and height of the seabed undulation for all the studied cases.

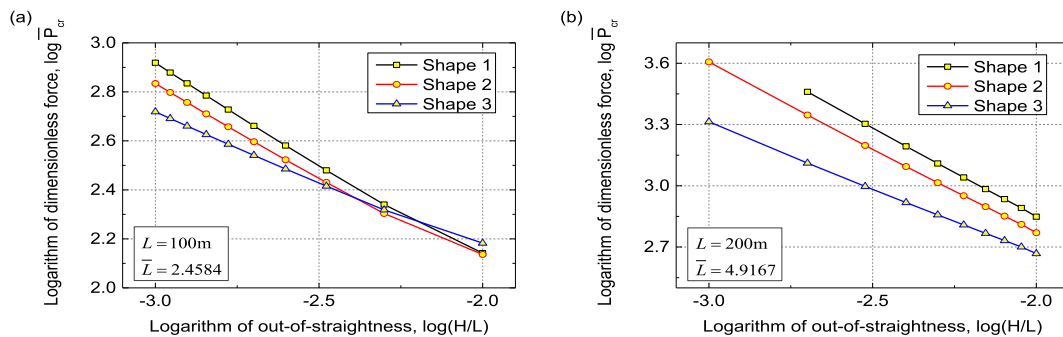


Fig. 14. The linear relationship between the OOS and the critical axial force in logarithmic form with (a) $L = 100$ m and (b) $L = 200$ m.

4.2. Fitting formulas of P_{cr}

So far, for each seabed shape, four series of results (with a total number of 36) are obtained. Based on the numerical results, the coefficients in Eqs. (10) and (11) are obtained via multiple linear regression analysis. The fitting formulas of the critical axial forces with the three seabed shapes are presented as below.

For shape 1

$$P_{cr1} = 0.2974 \left(\frac{L^3 q}{EI} \right)^{0.8351} \left(\frac{H}{L} \right)^{-0.8228} \frac{EI}{L^2} \tag{12}$$

For shape 2

$$P_{cr2} = 0.4231 \left(\frac{L^3 q}{EI} \right)^{0.7785} \left(\frac{H}{L} \right)^{-0.7685} \frac{EI}{L^2} \tag{13}$$

For shape 3

$$P_{cr3} = 1.7471 \left(\frac{L^3 q}{EI} \right)^{0.5989} \left(\frac{H}{L} \right)^{-0.5951} \frac{EI}{L^2} \tag{14}$$

The above equations are compared with the VFIFE results in Fig. 16. Although the fitting equations agree well with the original data, if the dimensional analysis in the previous section is proper, Eqs. (12)–(14) must be applicable for cases with different type of pipes. Therefore, in the next section, the above equations will be compared with results from different pipes. Moreover, the application scope and the relative errors of the above equations will be specified.

4.3. Application and error analysis

In this section the application scope of Eqs. (12)–(14) will be determined. Fig. 17(a) shows a pipeline in continuous contact with the foundation undulation. For the case with relatively short undulation, the pipeline is in partially contact with the foundation as shown in Fig. 17(b). Because the seabed is rigid in the numerical model, a pipeline in partially contact with the foundation would only contact with the rigid foundation at the peak point (see Fig. 17(b)). A partially contact situation can thus be simplified as the point contact situation as shown in Fig. 17(c). The deformation and stress distribution of a point-supported pipeline is almost the same with those of a partially-supported pipeline. Following previous studies (Croll, 1997; Liu et al., 2012a; Taylor and Tran, 1996), the deformation length L_d of a pipeline in point contact with the foundation is obtained as:

$$L_d = 5.826 \sqrt[4]{EIH/q} \tag{15}$$

With the pre-mentioned assumption, the deformation length of a pipeline in partially contact situation is also expressed as Eq. (15). In the partially contact situation, the pipeline deformation length L_d is longer than the undulation length L . In the continuous contact situation, the pipeline deformation length L_d equals to L . Therefore, the critical condition between the continuous contact situation and the partially contact situation is obtained as Eq. (16), which is also the expression of the

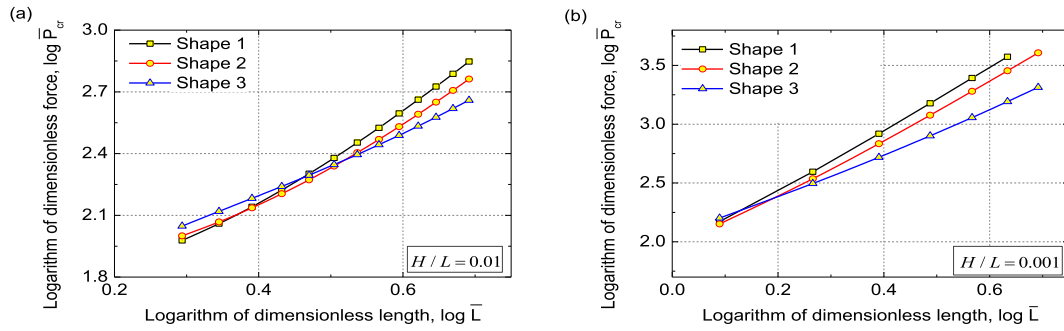


Fig. 15. The linear relationship between the non-dimensional undulation length and critical axial force in logarithmic form with (a) $H/L = 0.01$, and (b) $H/L = 0.001$.

critical undulation length L_{cr} .

$$L_{cr} = 5.826 \sqrt[4]{EIH/q} \tag{16}$$

Raise both sides of the equation to the fourth power and then divide

them by $L_{cr}EI/q$, we get

$$L_{cr}^3 \frac{q}{EI} = 1152 \frac{H}{L_{cr}} \tag{17}$$

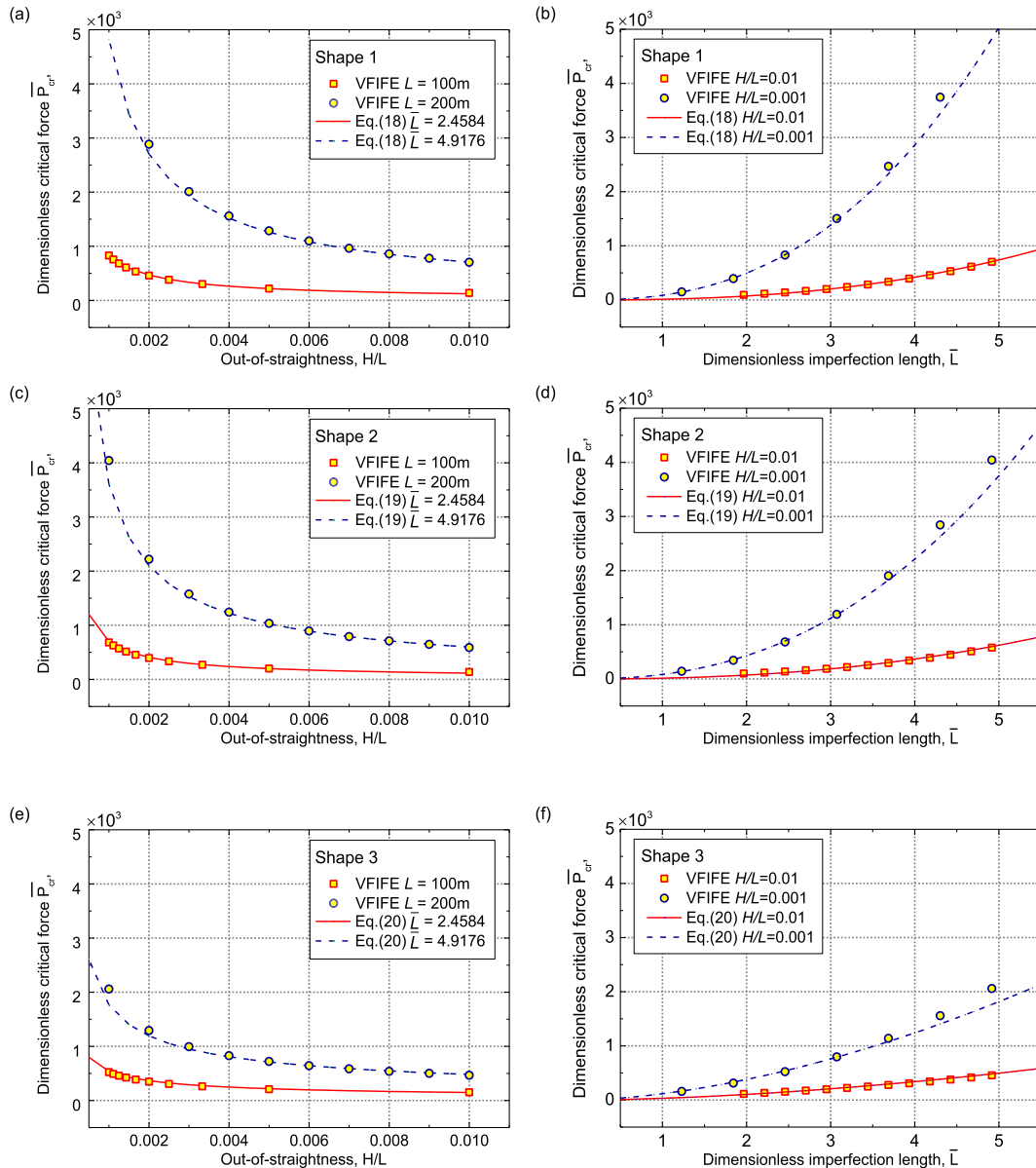


Fig. 16. Comparison between the fitting formulas and the simulation results: (a) shape 1 with $L = 100$ m and $L = 200$ m, (b) shape 1 with $H/L = 0.01$ and $H/L = 0.001$, (c) shape 2 with $L = 100$ m and $L = 200$ m, (d) shape 2 with $H/L = 0.01$ and $H/L = 0.001$, (e) shape 3 with $L = 100$ m and $L = 200$ m, (f) shape 3 with $H/L = 0.01$ and $H/L = 0.001$.

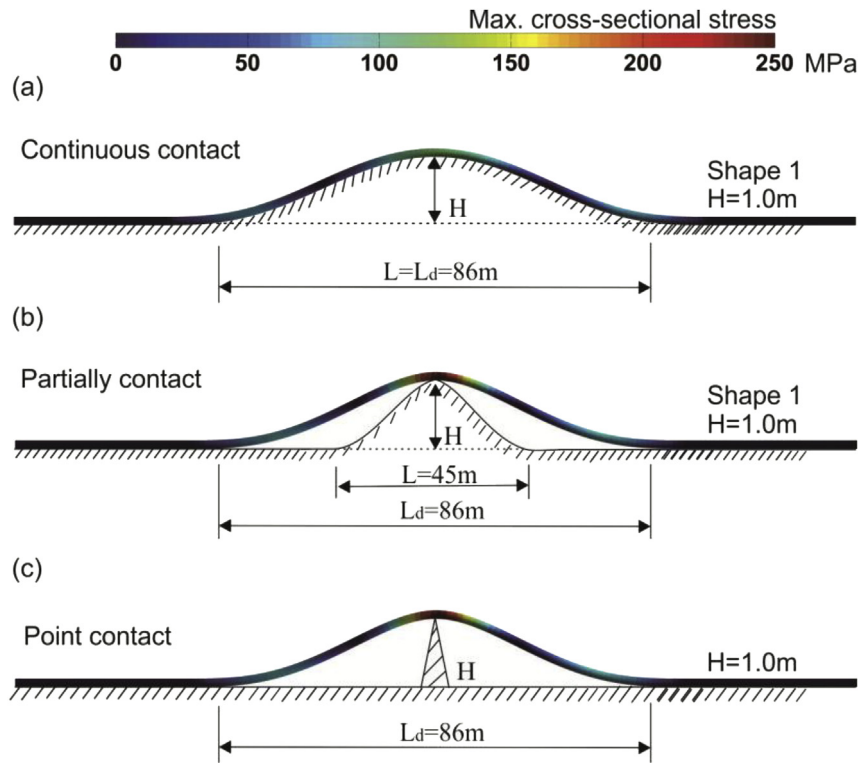


Fig. 17. Schematic diagram of a pipeline (a) in continuous, (b) partially, and (c) point contact with the foundation.

Considering Eq. (8), we get the dimensionless form of the above equation as:

$$\bar{L}_{cr} = \sqrt[3]{1152(H/L)_{cr}} \quad (18)$$

Similarly, the critical OOS between the continuous contact situation and the partially contact situation is

$$\left(\frac{H}{L}\right)_{cr} = \bar{L}_{cr}^3 / 1152 \quad (19)$$

Table 3
Parameters of the pipes used in application simulations.

Property	Value	
	Double-walled natural gas pipe	Single-walled crude oil pipe
The outer diameter of the steel pipe, D (mm)	522	385
The thickness of the steel pipe wall, t (mm)	14.3	12.0
The thickness of the outer concrete coating, t_o (mm)	40	0
The Young's modulus, E (GPa)	207	207
The Poisson's ratio, ν	0.3	0.3
The equivalent cross-sectional moment of inertia, I (m ⁴)	1.10×10^{-3}	2.22×10^{-4}
The equivalent cross-sectional area, A (m ²)	0.0222	0.0136
The density of pipe steel, ρ_s (kg/m ³)	7800	7800
The density of the outer concrete coating, ρ_c (kg/m ³)	3044	-
The density of seawater (kg/m ³)	1025	1025
The density of internal flow, ρ (kg/m ³)	149.0	800.0
The distributed load (submerged weight) per unit length, q (N/m)	1296.4	699.3
The thermal expansion coefficient, α_s (/°C)	1.17×10^{-5}	1.17×10^{-5}

Although the critical condition between the continuous and partially contact situations may differ for different seabed shapes, in this paper, the difference is ignored for simplicity.

Coefficients in Eqs. (12)–(14) are obtained with results from simulations with one type of pipe. In this section, the formulas are compared with results from simulations with pipelines with different properties listed in Table 3. One is a natural gas pipe, the outer diameter and wall thickness of the inner steel pipe are 0.522 m and 14.3 mm, respectively. Thickness of the outer concrete coating is 40 mm. Another one is a single-walled crude oil pipe with outer diameter of 0.385 m and wall thickness of 12.0 mm. Density of the natural gas and the crude oil are 149 kg/m³ and 800 kg/m³, respectively. The submerged weight of a pipeline includes gravity of the pipe wall, gravity of the internal flow and the buoyancy applied on the pipeline. According to the parameters listed in Table 3, the submerged weight is determined as 1296.4 N/m and

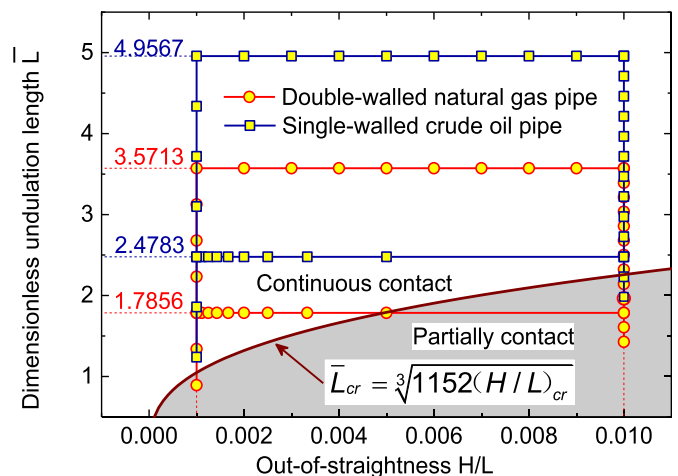


Fig. 18. The non-dimensional undulation length and height for the simulations with each seabed shape.

Table 4
The VFIFE results of the critical axial forces with the doubled-wall natural gas pipe and the singled-walled crude oil pipe.

Case parameters			Critical axial force P_{cr} (kN)					
No.	Height H (m)	Length L (m)	Doubled-walled natural gas pipe			Single-walled crude oil pipe		
			Shape 1	Shape 2	Shape 3	Shape 1	Shape 2	Shape 3
2	0.9	90	2336	2300	2451	646	618	768
3	1	100	1993	1914	2259	631	593	714
4	1.1	110	1807	1701	2117	587	557	635
5	1.2	120	1661	1597	1999	634	592	642
6	1.3	130	1633	1546	1888	646	591	616
7	1.4	140	1604	1520	1804	657	593	593
8	1.5	150	1598	1529	1736	674	601	579
9	1.5	150	1621	1530	1677	698	611	568
10	1.6	160	1646	1527	1628	721	623	560
11	1.7	170	1667	1529	1580	744	636	552
12	1.8	180	1692	1531	1544	769	649	544
13	1.9	190	1720	1546	1511	797	668	538
14	2	200	1764	1561	1490	832	686	536
15	1/9	100	7609	6733	6391	3517	2850	2220
16	0.125	100	6916	6169	5983	3161	2584	2074
17	1/7	100	6212	5598	5555	2811	2315	1911
18	1/6	100	5488	5007	5107	2452	2049	1749
19	0.2	100	4757	4398	4622	2100	1784	1567
20	0.25	100	4014	3770	4100	1745	1511	1375
21	1/3	100	3231	3111	3517	1371	1222	1163
22	0.5	100	2609	2604	2934	991	917	931
23	0.05	50	7127	7669	8718	2862	2700	2950
24	0.075	75	7343	6876	7454	3294	2867	2591
25	0.1	100	8301	7291	6783	3903	3271	2500
26	0.125	125	9399	7895	6431	4500	3580	2385
27	0.15	150	10,555	8572	6245	5102	3924	2364
28	0.175	175	11,714	9282	6152	5629	4185	2329
29	0.2	200	13,160	10,318	6325	–	4467	2298
30	0.4	200	7392	5960	4160	3344	2514	1480
31	0.6	200	5258	4324	3252	2352	1818	1141
32	0.8	200	4120	3447	2740	1829	1437	954
33	1	200	3418	2900	2402	1515	1207	829
34	1.2	200	2940	2523	2160	1291	1044	742
35	1.4	200	2592	2244	1975	1132	919	675
36	1.6	200	2324	2027	1828	1007	824	619
37	1.8	200	2113	1856	1708	910	748	574

699.3 N/m for the natural gas pipe and the crude oil pipe, respectively.

Same with the cases with the previous studied pipe, 36 simulations with the undulation length L and height H depicted in Fig. 13 are performed for each type of pipe. Eq. (18) or (19) is drawn in Fig. 18, together with the dimensionless undulation length and the OOS of all the simulations. The dimensionless length is respectively $\bar{L} = 1.7856$ for the gas pipe with the undulation length $L = 100$ m, $\bar{L} = 2.4783$ for the oil pipe with the undulation length $L = 100$ m, $\bar{L} = 3.5713$ for the gas pipe with the undulation length $L = 200$ m, and $\bar{L} = 4.9567$ for the oil pipe with the undulation length $L = 200$ m. The simulation points below the critical line represent the simulations in the partially contact situation. There are in total 9 cases in the partially contact situation.

Critical axial forces for all the simulation with the two types of pipe are listed in Table 4. The relative errors between Eqs. (12)–(14) and the VFIFE results are defined as

$$e = \frac{P_{cr}^{Eq} - P_{cr}^V}{P_{cr}^V} \times 100\% \quad (20)$$

where e is the relative error, P_{cr}^{Eq} is the critical force of the fitting formulas and P_{cr}^V is the critical force from the VFIFE simulations. The relative errors of formulas for the double-walled natural gas pipe and the single-walled crude oil pipe are depicted in Figs. 19 and 20. As shown in Fig. 18, when $\bar{L} = 2.4783$ (the single-walled crude oil pipe with the undulation length $L = 100$ m), $\bar{L} = 3.5713$ (the double-walled natural gas pipe with $L = 200$ m), and $\bar{L} = 4.9567$ (the single-walled crude oil pipe with the undulation length $L = 200$ m), the simulations are all in the continuous contact situation, correspondingly, the relative errors are shown in

Fig. 19(b)–(d), respectively. We can see the relative errors are all within the critical value of 10%. When $\bar{L} = 1.7856$ (the double-walled natural gas pipe with the undulation length $L = 100$ m), there are two simulations in the partially contact situation. The critical OOS when $\bar{L} = 1.7856$ is 0.0049, obtained with Eq. (19). As shown in Fig. 19(a), the relative errors in the continuous contact region are all within 10%, while the relative errors in the partially contact region decreases dramatically below -10% .

Similarly, the critical dimensionless length when the OOS $H/L = 0.01$ and $H/L = 0.001$ are respectively 2.2585 and 1.0483, obtained with Eq. (18). As shown in Fig. 20(a) and (b), for the simulations in the continuous contact situation, the relative errors are also within the range of $\pm 10\%$; for the simulations in the partially contact situation, the fitting errors decrease dramatically below -10% .

The upheaval buckling process of a pipeline in continuous contact with the foundation is different with that of a pipeline in partially contact with the foundation. This lead to the difference between the mechanical mechanisms and the dramatic variation of the relative errors. In this paper, the continuous contact situation is mainly concerned, therefore, we can make the summary that the fitting formulas are within the error range of $\pm 10\%$ for the OOS $H/L = 0.001$ to 0.01, the dimensionless undulation length $\bar{L} = 0.5$ to 5.0, and $L > L_{cr}$. Besides, the fitting formulas predict over-conservative critical axial forces for pipelines in partially contact situation.

5. Conclusion

In this paper, the VFIFE method is employed to study the upheaval

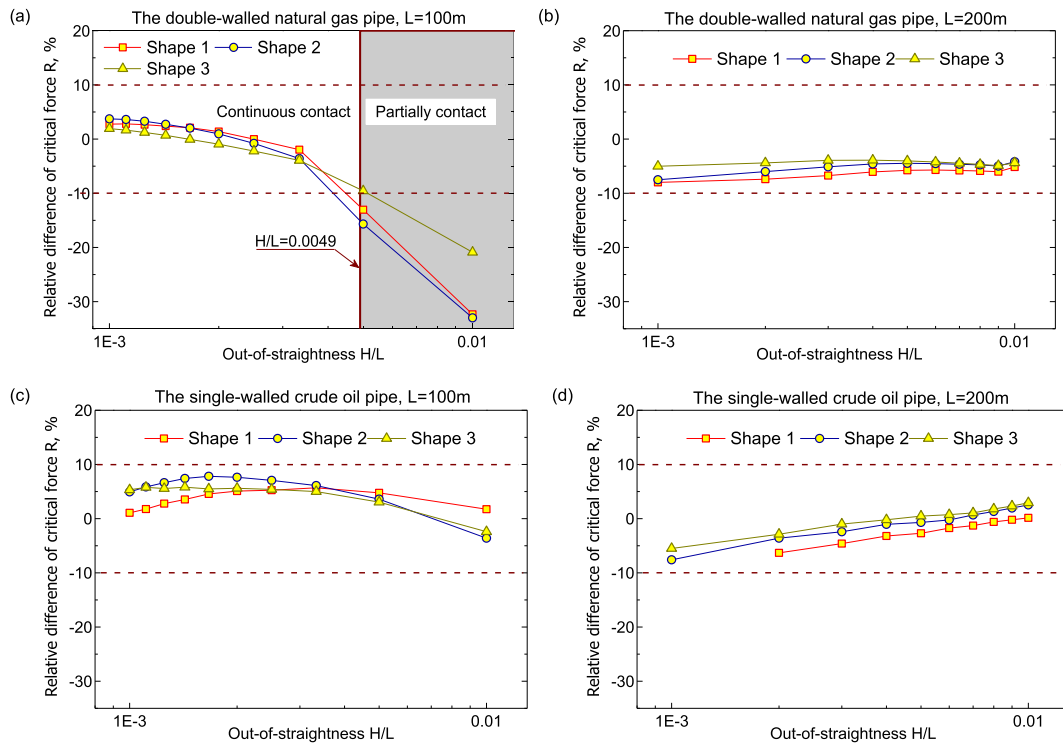


Fig. 19. The normalized differences between the simulation results and the fitting formulas: the double-walled natural gas pipe with (a) $L = 100$ m, and (b) $L = 200$ m; the single-walled crude oil pipe with (c) $L = 100$ m, and (d) $L = 200$ m.

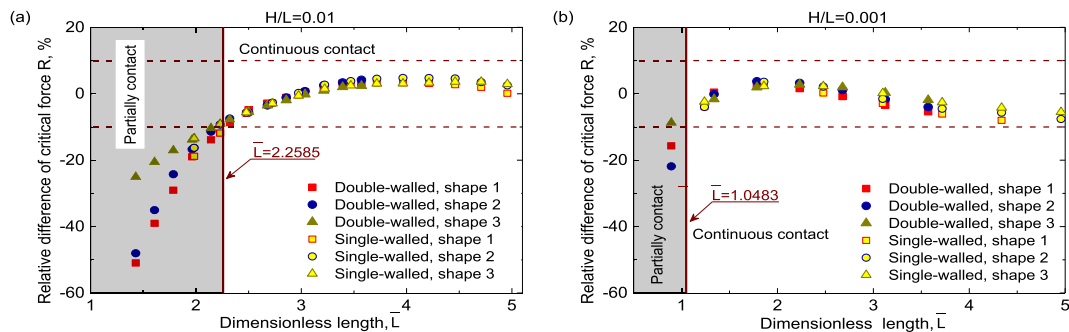


Fig. 20. The normalized differences between the simulation results and the fitting formulas: (a) $H/L = 0.01$, and (b) $H/L = 0.001$.

buckling behaviors of initially stressed pipelines laid on uneven seabed. The VFIFE model is proved as accurate as conventional FEM by comparing with the FEM results in previous research (Zeng et al., 2014). Numerical results shows that influence of the initial stress on the critical axial force is significant. The critical axial forces of a stressed pipeline segment is larger than that of an unstressed one. It is over-conservative to ignore the effect of the initial stress caused by the seabed undulation. Moreover, the relative difference caused by the initial stress increases with the OOS of the imperfection and the maximum value could reach at about 70%. Also, the relative difference is larger for more compacted undulation shape.

For initially stressed pipeline, the dimensionless critical axial force \bar{P}_{cr} is dominated by the dimensionless undulation length \bar{L} and the OOS H/L . With theory of dimensional analysis and numerous of numerical results, approximation formulas are obtained for three seabed undulation shapes. The formulas are proved applicable for different types of pipelines and within the error range of $\pm 10\%$ for pipelines in continuous contact situation ($\bar{L} > \bar{L}_{cr}$), within the application scope of the OOS from 0.001 to 0.01, the dimensionless undulation length from 0.5 to 5.0. For pipelines in partially contact situation, the proposed formulas of the critical axial force P_{cr} is over-conservative.

It should be noted that in this study, the pipeline is assumed to be elastic whilst it is suggested that the plastic effect might plays an important in the post-buckling stage. Moreover, length of the modeled pipeline hardly influence the critical condition of upheaval buckling but could significantly influence the post-buckling behaviors. Therefore, in further studies on the post-buckling behaviors, the plastic effect and influence of the length of the modeled pipeline must be considered.

Acknowledgments

This research was financially supported by the Key Instrument Developing Project of Chinese Academy of Sciences (No. ZDYZ2012-1-08-02), the National High-tech R&D Program of China (No. 2006AA09Z301) and the National Natural Science Foundation of China (No. 11302235).

References

Croll, J.G., 1997. A simplified model of upheaval thermal buckling of subsea pipelines. *Thin-walled Struct.* 29 (1), 59–78.
 Croll, J.G., 1998. A simplified analysis of imperfect thermally buckled subsea pipelines. *Int. J. Offshore Polar Eng.* 8 (04), 283–291.

- Fan, S., 2013. Upheaval Buckling of Offshore Pipelines. Department of Marine Technology. Norwegian University of Science and Technology, Trondheim.
- Guan, J., Nyström, P.R., Hansen, H.F., 2007. Optimized solutions to control lateral buckling of pipelines with snaked-lay: theoretical and numerical studies. In: ASME 2007 26th International Conference on Offshore Mechanics and Arctic Engineering. American Society of Mechanical Engineers, pp. 219–227.
- Guijt, J., 1990. Upheaval buckling of offshore pipelines: overview and introduction. In: Offshore Technology Conference. Offshore Technology Conference, pp. 573–580.
- Karampour, H., Albermani, F., Gross, J., 2013. On lateral and upheaval buckling of subsea pipelines. *Eng. Struct.* 52, 317–330.
- Liu, J., Xu, L., Lin, M., 2016a. Simulation of a buried pipeline crossing strike-slip fault based on Vector Form Intrinsic Finite Element (VFIFE) method with Fiber element model. In: The 26th International Ocean and Polar Engineering Conference. International Society of Offshore and Polar Engineers, Rhodes, Greece, pp. 977–983.
- Liu, R., Liu, W.-B., Wu, X.-L., Yan, S.-W., 2014a. Global lateral buckling analysis of idealized subsea pipelines. *J. Central South Univ.* 21, 416–427.
- Liu, R., Liu, W., Yan, S., Hong, Z., 2016b. Finite-element study of methods for triggering pipeline global buckling based on the concept of the perfect VAS length. *J. Pipeline Syst. Eng. Pract.* 7 (2), 04015027.
- Liu, R., Wang, W.-G., Yan, S.-W., Wu, X.-L., 2012a. Engineering measures for preventing upheaval buckling of buried submarine pipelines. *Appl. Math. Mech.* 33, 781–796.
- Liu, R., Xiong, H., Wu, X., Yan, S., 2014b. Numerical studies on global buckling of subsea pipelines. *Ocean. Eng.* 78, 62–72.
- Liu, Y., Li, X., Zhou, J., 2012b. Post-buckling studies on snaked-lay pipeline with new shape. *J. Inf. Comput. Sci.* 9 (12), 3315–3324.
- Maltby, T.C., Calladine, C.R., 1995a. An investigation into upheaval buckling of buried pipelines—I. Experimental apparatus and some observations. *Int. J. Mech. Sci.* 37 (9), 943–963.
- Maltby, T.C., Calladine, C.R., 1995b. An investigation into upheaval buckling of buried pipelines—II. Theory and analysis of experimental observations. *Int. J. Mech. Sci.* 37 (9), 965–983.
- O'Grady, R., Harte, A., 2013. Localised assessment of pipeline integrity during ultra-deep S-lay installation. *Ocean. Eng.* 68, 27–37.
- Palmer, A., Ellinas, C., Richards, D., Guijt, J., 1990. Design of submarine pipelines against upheaval buckling. In: Offshore Technology Conference. Offshore Technology Conference. OTC 6335.
- Richards, D., 1990. The Effect of Imperfection Shape on Upheaval Buckling Behaviour, *Advances in Subsea Pipeline Engineering and Technology*. Springer, pp. 51–66.
- Tan, Q.M., 2011. Dimensional Analysis-with Case Studies in Mechanics. Springer, Berlin Heidelberg.
- Taylor, N., Gan, A., 1987. Refined modelling for the vertical buckling of submarine pipelines. *J. Constr. Steel Res.* 7 (1), 55–74.
- Taylor, N., Gan, A.B., 1986. Submarine pipeline buckling—imperfection studies. *Thin-Walled Struct.* 4 (4), 295–323.
- Taylor, N., Tran, V., 1993. Prop-imperfection subsea pipeline buckling. *Mar. Struct.* 6 (4), 325–358.
- Taylor, N., Tran, V., 1996. Experimental and theoretical studies in subsea pipeline buckling. *Mar. Struct.* 9 (2), 211–257.
- Tian, Y., Cassidy, M.J., 2010. The challenge of numerically implementing numerous force–resultant models in the stability analysis of long on-bottom pipelines. *Comput. Geotechnics* 37 (1), 216–232.
- Tomes, K., Nystrem, P.R., Damsleth, P., Sortland, L.H., 1997. The behaviour of high pressure high temperature flowlines on very uneven seabed. In: The Seventh International Offshore and Polar Engineering Conference. International Society of Offshore and Polar Engineers, pp. 321–329.
- Wang, Z., Huachen, Z., Liu, H., Bu, Y., 2015. Static and dynamic analysis on upheaval buckling of unburied subsea pipelines. *Ocean. Eng.* 104, 249–256.
- Xu, L., Lin, M., 2014. Integrate pipe-soil interaction model with the vector form intrinsic finite element method-nonlinear analysis of free-span. In: The 24th International Ocean and Polar Engineering Conference. International Society of Offshore and Polar Engineers, Busan, Korea, pp. 72–79.
- Xu, L., Lin, M., 2017a. Analysis of buried pipelines subjected to reverse fault motion using the vector form intrinsic finite element method. *Soil Dyn. Earthq. Eng.* 93, 61–83.
- Xu, L., Lin, M., 2017b. Numerical modeling of the configuration of a long-distance free-spanning submarine pipeline on an uneven seabed. *Int. J. Offshore Polar Eng.* 27 (1), 102–111.
- Xu, L., Lin, M., 2017c. On the critical axial forces of upheaval buckling for imperfect submarine pipelines. *Eng. Struct.* 147, 692–704.
- Youssef, B.S., Cassidy, M.J., Tian, Y., 2013. Application of statistical analysis techniques to pipeline on-bottom stability analysis. *J. Offshore Mech. Arct. Eng.* 135 (3), 031701.
- Yun, H., Kyriakides, S., 1985. Model for beam-mode buckling of buried pipelines. *J. Eng. Mech.* 111 (2), 235–253.
- Zeng, X., Duan, M., Che, X., 2014. Critical upheaval buckling forces of imperfect pipelines. *Appl. Ocean Res.* 45, 33–39.
- Zhang, X., Duan, M., 2015. Prediction of the upheaval buckling critical force for imperfect submarine pipelines. *Ocean. Eng.* 109, 330–343.
- Zhu, J., Attard, M.M., Kellermann, D.C., 2015. In-plane nonlinear localised lateral buckling of straight pipelines. *Eng. Struct.* 103, 37–52.